Elastostatic loading of metallic glass-crystal nanocomposites: Relationship of creep rate and interface energy

Constanze Kalcher,[*] Tobias Brink ⬤,[†] Jochen Rohrer, Alexander Stukowski, and Karsten Albe

Institute of Materials Science, Technische Universität Darmstadt, Otto-Berndt-Str. 3, D-64287 Darmstadt, Germany

We study the creep behavior of $Cu_{64}Zr_{36}$ glass-crystal nanocomposites under elastostatic loading conditions in molecular dynamics simulations. By manipulating the glass-crystal interfaces of a precipitation-annealed glass containing Laves-type crystallites, we show that the creep behavior can be tuned. Specifically, we find that for the same microstructure the creep rate scales exponentially with the excess energy in the interfaces, which we raise artificially by disturbing the local short-range order in the atomistic model. The behavior shows analogies to Coble creep in crystalline metals, which depends on grain boundary diffusivity and implicitly on grain boundary energies.

I. INTRODUCTION

It is well established that crystalline nanoprecipitates in metallic glasses (MGs) induce limited plasticity [1–3] in this otherwise brittle material class. While the mechanical properties of metallic glass-crystal nanocomposites under conventional loading conditions at room temperature are well explored [2–6], their creep behavior under elastostatic loading conditions has not received much attention. Ceramic glass-matrix composites, in contrast, are already used in high-temperature applications. The presence of hard, crystalline particles in ceramic glasses is known to increase the viscosity and thus the creep resistance, which is usually rationalized by employing simple composite models [7–10].

In nanocrystalline metals, though, where grain boundaries have been found to behave glasslike in the limit of nanometer-sized grains [11–17], a significant influence of the grain boundary state on creep behavior [18–20] and plastic response [17,21] has been found in experiment and computer simulation. Moreover, simulations of irradiation-induced creep in nanocrystalline copper revealed that the creep rates are controlled by the amorphous grain boundary phase and that with decreasing grain sizes the creep behavior of the nanocrystalline material approaches the one observed for bulk amorphous materials [20].

These observations indicate that in glass-crystal nanocomposites with large specific interface areas the influence of the interface properties on the composite's mechanical behavior cannot be neglected. Indeed, recent experiments on silicon oxycarbide containing hard particles found a reduction of creep rates, which was not only dependent on the phase fraction but also on the nature of the interfaces [22]. In a previous study on metallic glass composites, we have shown that weak interfaces can act as preferential nucleation sites for shear transformations (STs) and may effectively *enhance* creep [23]. Thus, internal interfaces can reduce or enhance creep. This discrepancy is most likely an effect of the different interface states and fractions, and suggests that the state of the interface is a key parameter determining the creep behavior of glass-crystal composites, at least at large interface-to-volume ratios. The goal of the present work is thus to elucidate the influence of the interface state on the creep behavior of crystal-glass nanocomposites with high fractions of interfaces.

II. SIMULATION METHODS AND SETUP

We use the molecular dynamics simulation package LAMMPS [24] and an EAM potential by Mendelev *et al.* [25] to study a $Cu_{64}Zr_{36}$ MG matrix composite. All simulations use a timestep of 2 fs. First, a $Cu_{64}Zr_{36}$ MG sample of 63 108 atoms was produced by quenching from the melt with a cooling rate of $0.01\,\mathrm{K/ps}$. The composite sample was prepared by crystallization at temperatures close to the glass transition temperature T_g as described in Ref. [17]: The as-cast sample was annealed at $800\,\mathrm{K}$ for $t = 0.3\,\mu\mathrm{s}$ (sample A) and $t = 1.9\,\mu\mathrm{s}$ (sample B). Samples A and B were subsequently quenched to $50\,\mathrm{K}$ with $\dot{T} = 0.01\,\mathrm{K/ps}$. This process leads to the crystallization of Cu_2Zr Laves phases [17,26–31]. In that way, two composites with crystalline volume fractions $f_A = 6.9\%$ and $f_B = 29.0\%$ and different crystallite sizes have been generated. In addition, the as-cast sample was annealed for $1\,\mu\mathrm{s}$ at $580\,\mathrm{K} = 0.65T_g$ (sample C), which suppresses crystallization.

For our creep studies, we replicate these samples by $2 \times 2 \times 2$ to obtain larger composites of 504 864 atoms and dimensions of $20 \times 20 \times 20\,\mathrm{nm}^3$. Elastostatic tests were performed in the isothermal-isobaric ensemble at a constant uniaxial stress of $750\,\mathrm{MPa}$ and a temperature of $500\,\mathrm{K}$.

————————
[*]kalcher@mm.tu-darmstadt.de
[†]Present address: Civil Engineering Institute and Institute of Materials Science and Engineering, École polytechnique fédérale de Lausanne (EPFL), Station 18, CH-1015 Lausanne, Switzerland.
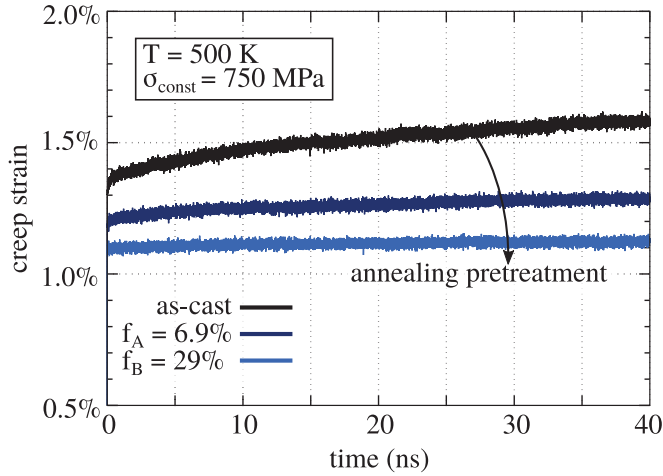
FIG. 1. Creep curves of a homogeneous metallic glass in the as-quenched state and after different annealing times at $T \approx T_g$. The samples contain different volume fractions of secondary phase, i.e., $f_A = 6.9\%$ and $f_B = 29\%$, depending on the duration of the annealing pretreatment. Sample B which has been annealed the longest shows the highest creep resistance.
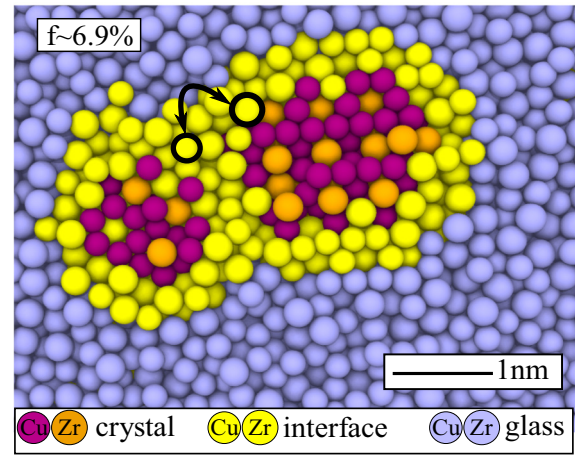

FIG. 2. Controlling the excess interface energy by interchange of atoms in the glass-crystal interphase. The figure shows a slice through two neighboring Cu_2Zr Laves phase crystallites embedded in a Cu-Zr glass matrix. The atoms in the glass-crystal interface region have been marked in yellow. In order to disturb the interface structure, the chemical identities of random Cu and Zr atoms within that region are interchanged.

III. RESULTS

A. Creep tests with and without secondary phases

The creep curves of the as-cast homogeneous $Cu_{64}Zr_{36}$ MG and of the samples after different precipitation annealing pretreatments are depicted in Fig. 1. The homogeneous as-cast glass exhibits an instant elastic strain of 1.3% and a total creep strain of 1.6% after 40 ns. In comparison, the composites are more creep resistant. The higher the crystalline phase fraction, the lower is the instant elastic response to the creep load and the creep rate. This is in contrast to our earlier work [23], where we always found an increase of creep rate. The specific interface areas are comparable to those used in this earlier work (ϕ between 200–400 μm^{-1} compared to $\phi_A = 301 \, \mu m^{-1}$ and $\phi_B = 856 \, \mu m^{-1}$). The interfaces in the present composite types, however, are in a deeper relaxation state because the crystallites have grown during the annealing pretreatment instead of being artificially implanted in the glass matrix. The latter procedure allows us to control the shape and phase fraction of the secondary phase and the specific glass-crystal interface area at the same time, but even after equilibration the resulting interfaces can still exhibit a large excess energy. In contrast, the annealing procedure yields very stable interfaces but does not allow us to adjust both the phase fraction and interface area. Moreover, the annealing pretreatment also leads to relaxation of the glass matrix. Thus both the glass-crystal interfaces and the glass matrix exhibit a deeper relaxation state than the as-cast glass (see also the analysis in Ref. [17]).

B. Influence of the interface state

In order to study the role of the glass-crystal interfaces in the composites' creep behavior, we need to ensure that the glass matrices are in comparable relaxation states, since the creep rates are influenced by all phases in the system. We thus chose sample A as a reference composite and manipulated the glass-crystal interface region by swapping the positions of random pairs of Cu and Zr atoms as shown in Fig. 2. In doing so, we gradually destroyed the well-relaxed state of the interface regions while ensuring that the local composition, the specific interface area, and the volume fraction of the secondary phase remain the same. We restricted the swapping modifications to glass atoms (i.e., noncrystalline atoms) that are located within a range of 5 Å of atoms belonging to a crystallite. Figure 2 depicts a slice through two neighboring Laves crystallites embedded in the glass matrix. An example of an atom swap is shown, i.e., the positions of a randomly chosen Cu-Zr atom pair in the yellow interface region are interchanged. Five different interface structures are created with varying degree of interface perturbation, where 5%, 10%, 15%, 25%, and 50% of Cu atoms in the interface have been swapped with Zr atoms. In the following we refer to them as samples A_1-A_5, with A_0 being the undisturbed sample.

After disturbing the chemical short range order (CSRO) as described, the samples are statically relaxed. We first probe the room-temperature mechanical response of samples A_0-A_5 under conventional loading conditions, i.e., strain-rate controlled tensile tests at $\dot{\epsilon} = 4 \times 10^7 \, s^{-1}$. The recorded stress-strain curves in Fig. 3(a) show that the yield stress is reduced from 3.2 GPa to 1.7 GPa. For the most severely manipulated interfaces, the typical stress overshoot observed in MGs disappears completely and the stress-strain curve resembles those observed for nanoglasses [32]. This is also reflected in the atomic-level shear strain [33] calculated for samples A_0 and A_5 [insets in Fig. 3(a)]. A transition in the deformation mode from shear band formation to a more homogeneous deformation can be observed for the interface-disturbed samples, which is in line with the expectation of the interface being in a higher energy state [34]. Moreover, the 500 K creep curves of these samples obtained under a constant applied elastostatic stress of 750 MPa are depicted in Fig. 3(b). As can be seen from the total creep strain value reached after 40 ns, disturbing
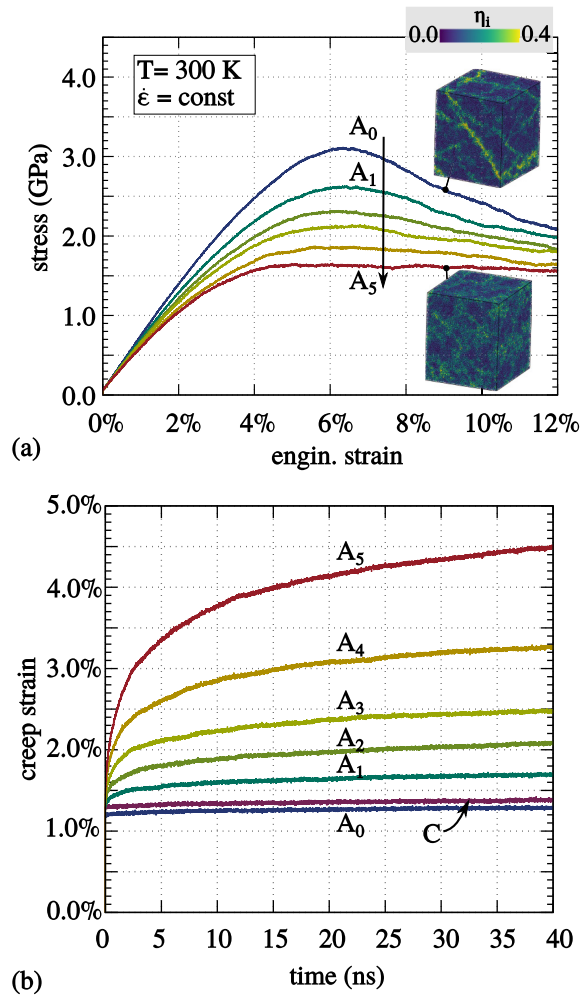
(a)

(b)

FIG. 3. (a) Uniaxial tensile tests at 300 K and constant engineering strain rate of the reference sample A_0 and the samples with differently disturbed interfaces A_1–A_5. The insets show snapshots of the atomic configurations at 12% macroscopic strain, color coded according to the atomic von Mises strain. (b) Uniaxial tensile creep tests at 500 K and constant applied load of 750 MPa of the same samples. For comparison, the creep behavior of sample C is shown, which has been annealed for 1 μs at 580 K, where no Laves precipitates nucleate.

the interface structure severely reduces the creep resistance of the composite material. Sample A_5, where 50% of all Cu atoms have been interchanged with Zr atoms, reaches a total strain of 4.5% after 40 ns. That is an increase by more than 3 percentage points of creep strain compared to the original annealed sample shown in dark blue. Such accelerated creep rates match the behavior reported in our earlier study that treated less relaxed glass-crystal interfaces [23].

Regarding the deformation mechanisms, all creep deformation in these composites is carried by the activation of STs [35,36] without percolation into shear bands, as visible in the von Mises shear strain field of composites A_0 and A_4 [Figs. 4(a) and 4(b)]. Two different color schemes have been used to be able to distinguish between atoms in the glass matrix and atoms that belong to either the crystallites or the glass-crystal interfaces. Creep in the present samples occurs by thermally activated events, which can be seen in

Fig. 4(a): The areas marked by red circles are structurally similar due to the $2 \times 2 \times 2$ replication of the original sample. Nevertheless, the shear events are independent, which they would not be if the simulation was in a stress-activated regime. When comparing the pristine composite sample A_0 to the composite A_4 with severely disturbed interfaces, it becomes evident that ST activity is facilitated in these disturbed regions, which explains the increased creep rates of A_1–A_5. As observed before in the context of thermal processing of MGs [37,38], stringlike atomic rearrangements occur, which can be understood as collective movement of a chain of atoms [Fig. 4(c)]. This snapshot has been taken in the secondary creep regime ($t = 38$ ns). Only those atoms are visible that have been displaced more than 2 Å in a 200 ps time window and are a neighbor to at least one other atom that has moved more than 2 Å. A cutoff of $r_c = 3.6$ Å has been chosen as a neighbor criterion, which is the average next-nearest neighbor distance in $Cu_{64}Zr_{36}$. In that way, we could detect stringlike chains composed of up to 10 collective atomic jumps.

As a reference, we also tested sample C, which has been annealed for 1 μs at only $0.65T_g$ to suppress crystallization. It exhibits creep rates close to those of sample A_0 [see Fig. 3(b)] and less than the as-cast glass. When comparing the creep behavior and mechanisms of the different samples, it becomes clear that on the one hand the creep resistance can be effectively increased by particle reinforcement, but also that the relaxation state of the amorphous phase strongly influences creep behavior. Any particle-reinforcing effect is quickly canceled out when disturbing the CSRO in the interfaces. This can again be compared to the situation in nanoglasses, where the disturbed glass-glass interfaces lead to a reduced strength, which can (at least in theory) be compensated by reinforcing these interfaces [39]. It is therefore necessary to characterize the state of the relaxed and damaged interfaces in more detail.

C. Connection to structural parameters

In order to measure the degree of damage introduced by disturbing the CSRO, the annealed and manipulated samples are characterized by means of their atomic Voronoi indices $\langle n_3, n_4, n_5, n_6 \rangle$, where n_i indicates the number of i-edged facets in the Voronoi cell given by the next nearest neighbor atoms [40–42]. We use the Voronoi analysis implemented in OVITO [43]. The Voronoi statistics of the undisturbed sample A_0 and samples A_4 and A_5 are shown in Fig. 5. We distinguish between atoms in three different phases: glass matrix, crystallites, and interfaces. Only the Voronoi indices that account for more than 2% of the atoms in either the interface phase or the glass matrix are shown. In the following we adopt the nomenclature commonly used in the literature which distinguishes between the geometrically favored clusters of a certain coordination, the so-called Z clusters, and the distorted polyhedra with the same coordination number (CN) [44–46]. In the reference sample, the population of polyhedra larger than the threshold value is actually very similar within the interface and glass phases. This again speaks for the fact that the interface structure is well relaxed. Moreover, in all samples, the Cu-centered Z12 cluster remains the most
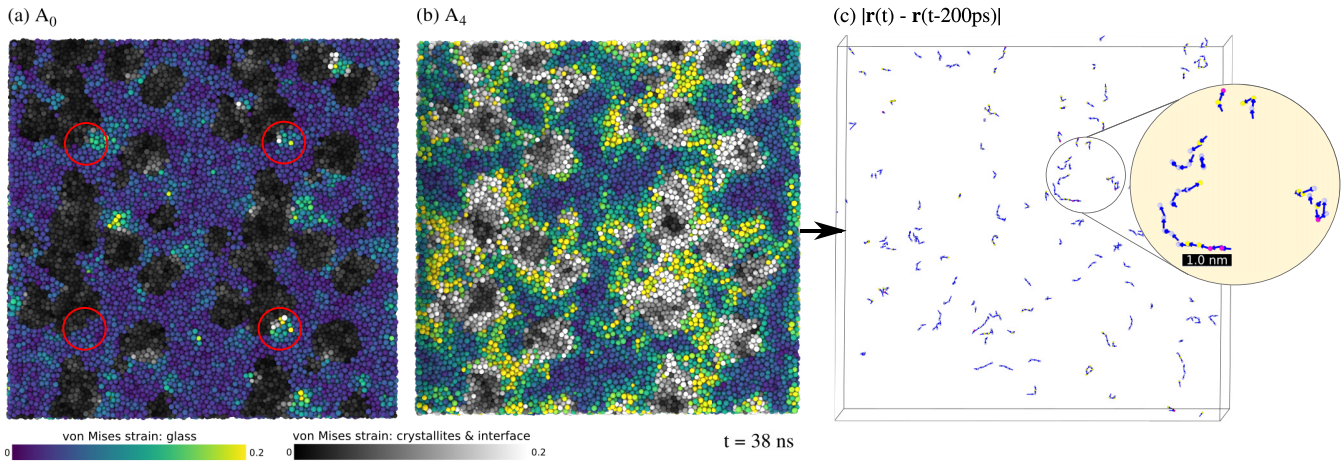
(a) A$_0$ (b) A$_4$ (c) |**r**(t) - **r**(t-200ps)|

von Mises strain: glass   von Mises strain: crystallites & interface

0 — 0.2   0 — 0.2   t = 38 ns

FIG. 4. Snapshots of samples (a) A$_0$ and (b) A$_4$ in the secondary creep regime ($t = 38$ ns) where the atoms are color coded by their local von Mises shear strain (with reference to $t = 0$ ns). Two different color schemes have been used to discriminate between atoms in the glass matrix and atoms belonging to the crystallites and the glass-crystal interfaces. The red circles mark regions that are structurally equivalent due to the $2 \times 2 \times 2$ replication of the smaller, annealed sample before the creep test. The ST events in these regions are independent, which indicates that they are thermally activated. (c) Displacement vectors calculated within a time window of 200 ps. Only those atoms are shown that have moved more than 2 Å and also have an immediate neighbor (within a distance of $r_c = 3.6$ Å) that has moved more than 2 Å. Stringlike excitations are observed.

prominent structural motif in the glass matrix, followed by its slightly distorted version, the $\langle 0, 2, 8, 2 \rangle$ polyhedron. The compatibility between the crystal and glass structures enables this favorable structure: The copper atoms in the Laves phases are also centers of Z12 icosahedra. This explains why the interface in the undisturbed sample is quite stable and why such small crystallites do not dissolve, which would be expected for less compatible crystal structures, such as fcc [47].

The interface manipulation step mostly affects the population of Z12 clusters in the interface; it gets lower as more interface atoms are interchanged. Additional geometrically unfavored motifs with CN > 12 appear in the interface instead. A similar trend can be observed for the Zr-centered Voronoi polyhedra: The population of geometrically unfavored CN motifs is increasing at the cost of the population of Z clusters. In the pristine sample, the Zr-centered Z16 polyhedron with index $\langle 0, 0, 12, 4 \rangle$ is the most prominent motif in the interface. That means most of the Zr atoms in the interface also possess the same coordination as in the Laves phase.

For comparison, Fig. 5 also includes the Voronoi statistics of sample C, which exhibits a similar structure profile as the glass matrix of the heterogeneous samples but contains a smaller fraction of full icosahedra. This shows that the two thermal processing routes—annealing close T_g and annealing well below T_g—lead to different relaxation states of the glass. It is important to note that the glass matrices in sample set A are thus not directly comparable to the homogeneous case C.

Moreover, we have characterized the different phases in terms of their stiffness by calculating the local shear moduli. More specifically, in MD simulations of MGs, the lowest per-atom Kelvin shear modulus [48,49] G_1 has been used to characterize the glass in terms of its relaxation state [17,50,51]. The distributions of the per-atom shear moduli G_1 in the different composite phases are given in Fig. 6. The blue curves correspond to the untreated sample A$_0$. It is evident that the crystallites are stiffer than the glass matrix and that

the interfaces exhibit values in between those of the matrix and the crystallites. This corroborates the reinforcing effect observed in Fig. 1(b). However, after disturbing the interfaces this situation changes: While the atoms in the glass matrix are only weakly affected, the distribution of atomic shear moduli in the interface clearly shifts to lower values and indicates a softening of the interface. Interestingly, even the crystallites appear to be affected by the interface manipulation. This is most probably due to their small size. Since they have a mean diameter of only 1.5 nm, disturbance of the interface can affect values within the crystallites due to the finite range of atomic interactions.

D. Connection to vibrational properties

In addition to structural and mechanical parameters, the relaxation state of amorphous materials has also been connected to their vibrational properties [52–58]. The vibrational density of states $g(\nu)$ exhibits an excess of states at a frequency of around $\nu = 1$ THz compared to crystalline materials—called "boson peak" for historical reasons [59]—which is clearly visible as a peak when plotting $g(\nu)/\nu^2$. While the origin of this phenomenon has been under discussion for many years [51,52,59–70], most authors agree that it is related to "disorder" or "defects" in some way [45,50–53,57,59–63,65,66,69,70]. Indeed, the height of this peak [defined as the maximum of the $g(\nu)/\nu^2$ curve or the equivalent in the heat capacity over temperature curve] has been found to increase with different disorder parameters [45,57,59,63,66,70], which is corroborated by studies reporting a high boson peak signal in structurally severely disturbed shear bands in bulk glasses [54,55]. Moreover, this heightened signal decreases again with subsequent annealing [54,55]. The present system is thus an interesting example case to probe the connection between the boson peak, defective glass structures, and nonlinear mechanical response, such as creep.
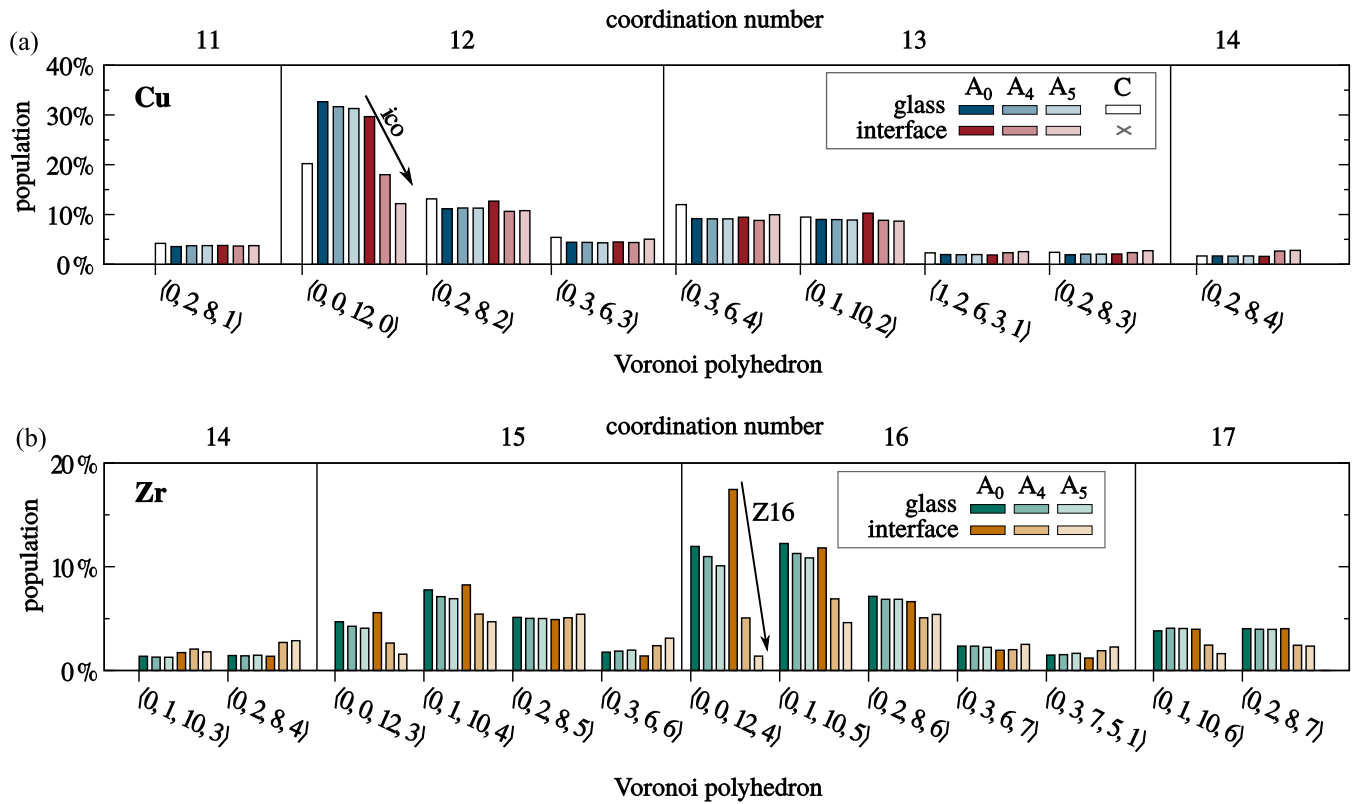
FIG. 5. Statistics of the (a) Cu-centered and (b) Zr-centered Voronoi polyhedra that occur more often than 2% either in the glass or the interface phase. The plots compare the reference sample A_0 to samples A_4 and A_5, where 25% and 50% of the Cu atoms in the glass-crystal interface have been interchanged with Zr atoms. (a) Compared to A_0, the fraction of Z12 clusters (icosahedral clusters) in samples A_4 and A_5 is mainly reduced in the interfaces but also in the glass matrix. For comparison, the homogeneous sample C is included in the Voronoi statistics of Cu-centered polyhedra. (b) The Zr-centered Z16 clusters with index $\langle 0, 0, 12, 4 \rangle$ behave similarly. Since these clusters also occur in the Laves phase, their fraction is higher in the relaxed interface than in the bulk glass.

We calculated $g(\nu)$ separately for the crystallites, interfaces, and glass matrix with the same procedure described in Ref. [51]. As a result of the phase separation during crystallization, the sample sets A, B, and C are not directly

FIG. 6. Softening of the samples with disturbed interfaces. The graph shows the distribution of the lowest per-atom Kelvin shear moduli G_1 in the glass matrix, interface, and crystal phases. The crystallites are so small that they are also softened when the interface regions are manipulated.

comparable due to their slightly different compositions and the different confinement of the amorphous phase by the abutting crystallites. In addition, the reduced representation of the data by multiplication with a ν^{-2} term makes the apparent height of the boson peak susceptible to frequency shifts of the vibrational spectrum, e.g., due to different densities of the material. We therefore limit our discussion to sample set A. As expected [66], the boson peak signal is increased and slightly shifted to lower frequencies with an increasing number of defects and vice versa [Fig. 7(a)]. We can again see that the amorphous matrix is also affected by the damaged interface.
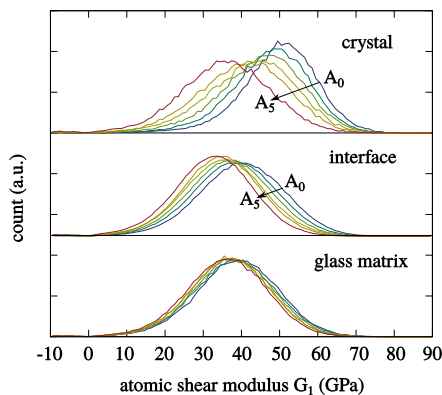
Figure 7(b) shows that there is a direct, linear relation between the elastic properties, the boson peak, and the excess energy introduced by disturbing the CSRO. This confirms that the boson peak is a probe for excess energy/enthalpy [52,58] and elastic softening [53,57,59,65]. Interestingly, while both G_1 and the boson peak are probes for the elastic response of the system and the boson peak is thought to be related to β relaxation processes [71], our results demonstrate that these quantities are also clearly correlated with the creep rate, which can be understood as the rate for larger, irreversible transitions in the potential energy landscape.
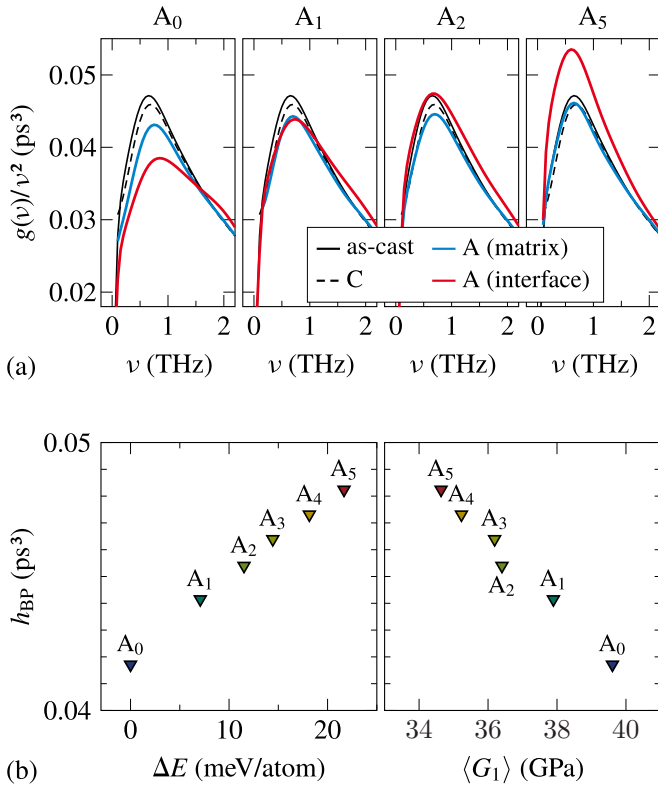
FIG. 7. (a) Comparison of the boson peak in the as-cast and annealed (sample C) glasses with the composites (sample set A). The contributions in the composites are split into the interface region and the glass matrix. (b) The height h_{BP} of the boson peak, defined as the maximum of the g/ν^2 curve, as a function of the excess energy ΔE and the median per-atom Kelvin shear modulus G_1 (data for the complete amorphous phase, i.e., interface and matrix). A clear correlation between structural and mechanical relaxation parameters and the excess vibrational modes can be observed.

IV. RELATION TO COBLE CREEP

As we have seen above, randomly manipulating the chemical short range order of the glass-crystal interfaces, as done in this study, changes their energetic state by introducing excess energy. In nanocrystalline materials, grain boundary diffusion can contribute to creep deformation (Coble creep). From this class of materials, it is already known that there is a correlation between the interface energy γ and the self-diffusion coefficients in the lattice D_{lat} and grain boundaries D_{GB}, respectively [72,73]:

$$D_{GB} = D_{lat} \exp\left(\frac{\gamma}{\rho k_B T}\right), \qquad (1)$$

which means that for vanishing interface energies, D_{GB} converges to D_{lat}.

Since the diffusion coefficient should be proportional to the creep rate (we can preclude dislocation activity in our crystalline nanoparticles), it is tempting to relate the relative creep rates of the disturbed composites, $\dot{\epsilon}_{dist}/\dot{\epsilon}_{ref}$, to the interface energy, analogous to Eq. (1). This is valid under the assumption that only the interface phase and the glass
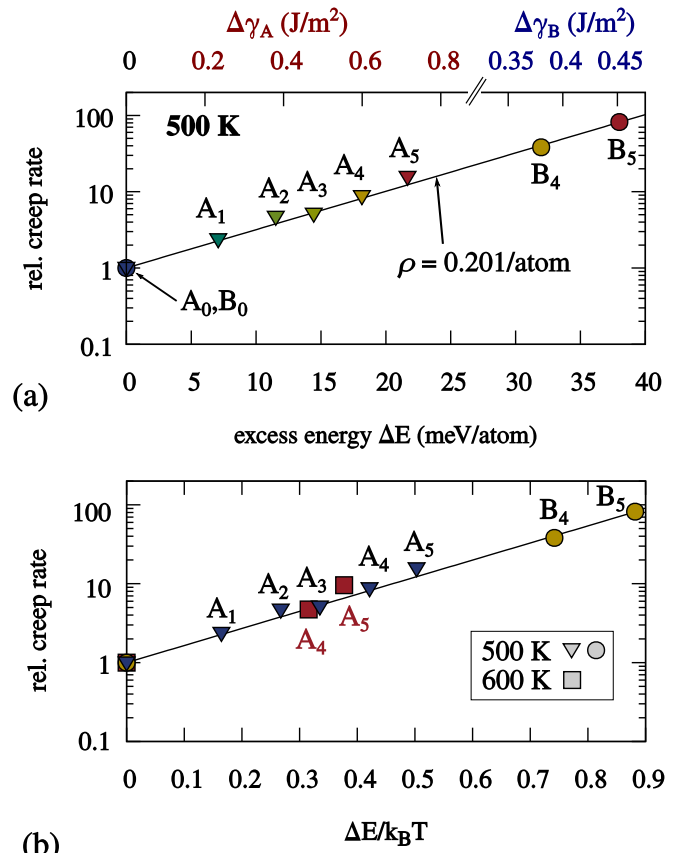

FIG. 8. (a) Relative creep rates obtained at 500 K vs excess energy for all samples. Excess energies in units of meV/atom can be converted into excess interface energies $\Delta\gamma$ in J/m^2 using the glass-crystal interface areas in the composites. The line shows the best fit for Eq. (3) at 500 K. (b) Two more creep rates obtained at 600 K have been added. When the excess energy is scaled with the creep temperature, the data follows the same master curve as in (a).

matrix show viscous flow around the stiff Laves-phase grains. Creep rates have been linearly fitted in the transient creep regime between $t = 15$ ns and $t = 40$ ns for all samples. Moreover, we define the excess energy ΔE as the potential energy difference between the disturbed and the reference sample:

$$\Delta E = \frac{\left(E_{pot}^{dist} - E_{pot}^{ref}\right)}{N}, \qquad (2)$$

where N is the total number of atoms in the sample. The excess energy is thus attributed to all atoms in the system, not just those in the interface region. In our case, due to the close spacing of the crystallites, the damage is not confined to the interface but affects the whole sample volume, as already indicated by the distribution of G_1 shown in Fig. 6 and the boson peak in Fig. 7. Avoiding such "crosstalk" would require much larger crystallite sizes and also larger interspacings between them. Figure 8(a) shows the correlation of the relative creep rates with the excess interface energy. Indeed, the data follow an exponential scaling law similar to

the grain boundary diffusion model given in Eq. (1):

$$\dot{\epsilon}_{\text{dist}}/\dot{\epsilon}_{\text{ref}} = \exp\left(\frac{\Delta E}{\rho k_B T}\right). \tag{3}$$

We repeated the above analysis with sample B, which differs in terms of the relaxation state of the glass and the interface, as well as crystallite number and size. As shown in Fig. 8(a), the creep enhancement follows the same curve predicted by sample A, which means that the interface-related excess energy is a good predictor of creep rates.

The fit curve in Fig. 8(a) was obtained for creep data with a constant temperature (500 K) and stress (750 MPa). In order to confirm the thermal activation model underlying Eq. (3), we repeated the experiments for samples A_0, A_4, and A_5 at a 20% increased temperature of 600 K and fitted the creep rates again. When the excess energies on the abscissa are scaled with $1/k_B T$, the additional data points fall on one master curve with the 500 K data, corresponding to $\rho = 0.201/\text{atom}$ as well [Fig. 8(b)].

The advantage of the definition of excess energy in Eq. (2) is that no assumption about the exact position and width of the interphase had to be made. Still, in order to relate this to a more classical description in terms of an excess interface energy $\Delta\gamma$, we can use an approximated interface area A_{int} which is calculated using the surface reconstruction algorithm implemented in OVITO [43,74]. With the interface areas of 2431 nm^2 (sample A) and 6883 nm^2 (sample B) and

using $\Delta\gamma = N\Delta E/A_{\text{int}}$, we obtain the excess interface energies indicated on the top of Fig. 8(a). These excess energies roughly match the ones expected for grain boundaries, which are typically on the order of 1 J/m^2.

V. CONCLUSION

By starting from a metallic glass composite with well-relaxed crystal-glass interfaces, we found that the initially relatively low creep rate can be increased by systematically disturbing the CSRO of these interfaces. The resulting excess energy of the interface state can be linked directly to typical structural parameters, such as the degree of icosahedral short-range order, but also to local elastic constants and vibrational properties ("boson peak"). Most importantly, though, we found that the creep rate is a function of the excess interface energy, following an exponential law analogous to grain boundary diffusion models. This means that high-energy interfaces can negatively impact the macroscopic creep performance, while composites with better relaxed interfaces can benefit from creep-reducing effects of the inclusions.

[1] H. Ma, J. Xu, and E. Ma, Mg-based bulk metallic glass composites with plasticity and high strength, Appl. Phys. Lett. **83**, 2793 (2003).

[2] J. Eckert, J. Das, S. Pauly, and C. Duhamel, Mechanical properties of bulk metallic glasses and composites, J. Mater. Res. **22**, 285 (2007).

[3] A. L. Greer, Shear bands in metallic glasses, Mater. Sci. Eng., R **74**, 71 (2013).

[4] C. C. Hays, C. P. Kim, and W. L. Johnson, Microstructure Controlled Shear Band Pattern Formation and Enhanced Plasticity of Bulk Metallic Glasses Containing in Situ Formed Ductile Phase Dendrite Dispersions, Phys. Rev. Lett. **84**, 2901 (2000).

[5] C. C. Hays, C. P. Kim, and W. L. Johnson, Improved mechanical behavior of bulk metallic glasses containing in situ formed ductile phase dendrite dispersions, Mater. Sci. Eng., A **304–306**, 650 (2001).

[6] T. Brink, M. Peterlechner, H. Rösner, K. Albe, and G. Wilde, Influence of Crystalline Nanoprecipitates on Shear-Band Propagation in Cu-Zr-Based Metallic Glasses, Phys. Rev. Appl. **5**, 054005 (2016).

[7] A. R. Boccaccini, On the viscosity of glass composites containing rigid inclusions, Mater. Lett. **34**, 285 (1998).

[8] T. Rouxel, B. Baron, P. Verdier, and T. Sakuma, SiC particle reinforced oxynitride glass: Stress relaxation, creep and strain-rate imposed experiments, Acta Mater. **46**, 6115 (1998).

[9] T. Rouxel, G.-D. Soraru, and J. Vicens, Creep viscosity and stress relaxation of gel-derived silicon oxycarbide glasses, J. Am. Ceram. Soc. **84**, 1052 (2001).

[10] C. Stabler, F. Roth, M. Narisawa, D. Schliephake, M. Heilmaier, S. Lauterbach, H.-J. Kleebe, R. Riedel, and E. Ionescu, High-temperature creep behavior of a SiOC glass ceramic free of segregated carbon, J. Eur. Ceram. Soc. **36**, 3747 (2016).

[11] C. A. Schuh, T. G. Nieh, and H. Iwasaki, The effect of solid solution W additions on the mechanical properties of nanocrystalline Ni, Acta Mater. **51**, 431 (2003).

[12] A. C. Lund, T. G. Nieh, and C. A. Schuh, Tension/compression strength asymmetry in a simulated nanocrystalline metal, Phys. Rev. B **69**, 012101 (2004).

[13] A. S. Argon and S. Yip, The strongest size, Philos. Mag. Lett. **86**, 713 (2006).

[14] A. J. Detor and C. A. Schuh, Tailoring and patterning the grain size of nanocrystalline alloys, Acta Mater. **55**, 371 (2007).

[15] J. R. Trelewicz and C. A. Schuh, The Hall–Petch breakdown in nanocrystalline metals: A crossover to glass-like deformation, Acta Mater. **55**, 5948 (2007).

[16] M. Grewer and R. Birringer, Shear shuffling governs plastic flow in nanocrystalline metals: An analysis of thermal activation parameters, Phys. Rev. B **89**, 184108 (2014).

[17] T. Brink and K. Albe, From metallic glasses to nanocrystals: Molecular dynamics simulations on the crossover from glass-like to grain-boundary-mediated deformation behaviour, Acta Mater. **156**, 205 (2018).

[18] W. M. Yin and S. H. Whang, Creep in boron-doped nanocrystalline nickel, Scr. Mater. **44**, 569 (2001).

[19] J. Schäfer, Y. Ashkenazy, K. Albe, and R. S. Averback, Effect of solute segregation on thermal creep in dilute nanocyrstalline Cu alloys, Mater. Sci. Eng. A **546**, 307 (2012).

[20] Y. Ashkenazy and R. S. Averback, Irradiation induced grain boundary flow—a new creep mechanism at the nanoscale, Nano Lett. **12**, 4084 (2012).

[21] J. Hu, Y. N. Shi, X. Sauvage, G. Sha, and K. Lu, Grain boundary stability governs hardening and softening in extremely fine nanograined metals, Science **355**, 1292 (2017).

[22] C. Stabler, D. Schliephake, M. Heilmaier, T. Rouxel, H.-J. Kleebe, M. Narisawa, R. Riedel, and E. Ionescu, Influence of SiC/silica and carbon/silica interfaces on the high-temperature creep of silicon oxycarbide-based glass ceramics: A case study, Adv. Eng. Mater. **21**, 1800596 (2018).

[23] C. Kalcher, T. Brink, J. Rohrer, A. Stukowski, and K. Albe, Interface-controlled creep in metallic glass composites, Acta Mater. **141**, 251 (2017).

[24] S. Plimpton, Fast parallel algorithms for short-range molecular dynamics, J. Comp. Phys. **117**, 1 (1995), https://lammps.sandia.gov/.

[25] M. I. Mendelev, M. J. Kramer, R. T. Ott, D. J. Sordelet, D. Yagodin, and P. Popel, Development of suitable interatomic potentials for simulation of liquid and amorphous Cu–Zr alloys, Philos. Mag. **89**, 967 (2009).

[26] C. Tang and P. Harrowell, Predicting the solid state phase diagram for glass-forming alloys of copper and zirconium, J. Phys.: Condens. Matter **24**, 245102 (2012).

[27] J. Zemp, M. Celino, B. Schönfeld, and J. F. Löffler, Icosahedral superclusters in $Cu_{64}Zr_{36}$ metallic glass, Phys. Rev. B **90**, 144108 (2014).

[28] J. Zemp, M. Celino, B. Schönfeld, and J. F. Löffler, Crystal-Like Rearrangements of Icosahedra in Simulated Copper-Zirconium Metallic Glasses and their Effect on Mechanical Properties, Phys. Rev. Lett. **115**, 165501 (2015).

[29] C. C. Hays, C. P. Kim, and W. L. Johnson, Large supercooled liquid region and phase separation in the Zr–Ti–Ni–Cu–Be bulk metallic glasses, Appl. Phys. Lett. **75**, 1089 (1999).

[30] H. Men, S. J. Pang, and T. Zhang, Glass-forming ability and mechanical properties of $Cu_{50}Zr_{50-x}Ti_x$ alloys, Mater. Sci. Eng. A **408**, 326 (2005).

[31] It should be noted that while Laves phases are not observed at low temperature in pure Cu-Zr glasses and represent an artifact of the interatomic potential [26], such phases do play a role in more complex Cu-Zr-based glasses [29,30]. More importantly, the procedure employed in the present paper [17,27,28] leads to model systems that fulfill the requirements of being well relaxed and possessing a low interface energy but being only partially crystallized.

[32] D. Şopu, Y. Ritter, H. Gleiter, and K. Albe, Deformation behavior of bulk and nanostructured metallic glasses studied via molecular dynamics simulations, Phys. Rev. B **83**, 100202(R) (2011).

[33] F. Shimizu, S. Ogata, and J. Li, Theory of shear banding in metallic glasses and molecular dynamics calculations, Mater. Trans. **48**, 2923 (2007).

[34] Y. Q. Cheng, A. J. Cao, and E. Ma, Correlation between the elastic modulus and the intrinsic plastic behavior of metallic glasses: The roles of atomic configuration and alloy composition, Acta Mater. **57**, 3253 (2009).

[35] A. S. Argon, Plastic deformation in metallic glasses, Acta Metall. **27**, 47 (1979).

[36] A. S. Argon and L. T. Shi, Development of visco-plastic deformation in metallic glasses, Acta Metall. **31**, 499 (1983).

[37] Y. Ritter and K. Albe, Thermal annealing of shear bands in deformed metallic glasses: Recovery mechanisms in $Cu_{64}Zr_{36}$ studied by molecular dynamics simulations, Acta Mater. **59**, 7082 (2011).

[38] P. M. Derlet and R. Maaß, Thermal processing and enthalpy storage of a binary amorphous solid: A molecular dynamics study, J. Mater. Res. **32**, 2668 (2017).

[39] C. Kalcher, O. Adjaoud, J. Rohrer, A. Stukowski, and K. Albe, Reinforcement of nanoglasses by interface strengthening, Scr. Mater. **141**, 115 (2017).

[40] G. Voronoï, Nouvelles applications des paramètres continus à la théorie des formes quadratiques, J. Reine Angew. Math. **1908**, 97 (1908).

[41] G. Voronoï, Nouvelles applications des paramètres continus à la théorie des formes quadratiques, J. Reine Angew. Math. **1908**, 198 (1908).

[42] G. Voronoï, Nouvelles applications des paramètres continus à la théorie des formes quadratiques, J. Reine Angew. Math. **1909**, 67 (1909).

[43] A. Stukowski, Visualization and analysis of atomistic simulation data with OVITO – the Open Visualization Tool, Modell. Simul. Mater. Sci. Eng. **18**, 015012 (2010), https://ovito.org/.

[44] Y. Q. Cheng and E. Ma, Atomic-level structure and structure–property relationship in metallic glasses, Prog. Mater Sci. **56**, 379 (2011).

[45] J. Ding, S. Patinet, M. L. Falk, Y. Cheng, and E. Ma, Soft spots and their structural signature in a metallic glass, Proc. Natl. Acad. Sci. USA **111**, 14052 (2014).

[46] E. Ma, Tuning order in disorder, Nat. Mater. **14**, 547 (2015).

[47] T. Brink, D. Şopu, and K. Albe, Solid-state amorphization of Cu nanolayers embedded in a $Cu_{64}Zr_{36}$ glass, Phys. Rev. B **91**, 184103 (2015).

[48] W. Thomson, XXI. Elements of a mathematical theory of elasticity, Philos. Trans. R. Soc. London **146**, 481 (1856).

[49] K. Helbig, Review paper: What Kelvin might have written about elasticity, Geophys. Prospect. **61**, 1 (2013).

[50] P. M. Derlet, R. Maaß, and J. F. Löffler, The boson peak of model glass systems and its relation to atomic structure, Eur. Phys. J. B **85**, 148 (2012).

[51] T. Brink, L. Koch, and K. Albe, Structural origins of the boson peak in metals: From high-entropy alloys to metallic glasses, Phys. Rev. B **94**, 224203 (2016).

[52] T. S. Grigera, V. Martín-Mayor, G. Parisi, and P. Verrocchio, Phonon interpretation of the 'boson peak' in supercooled liquids, Nature (London) **422**, 289 (2003).

[53] A. N. Vasiliev, T. N. Voloshok, A. V. Granato, D. M. Joncich, Yu. P. Mitrofanov, and V. A. Khonik, Relationship between low-temperature boson heat capacity peak and high-temperature shear modulus relaxation in a metallic glass, Phys. Rev. B **80**, 172102 (2009).

[54] J. Bünz, T. Brink, K. Tsuchiya, F. Meng, G. Wilde, and K. Albe, Low Temperature Heat Capacity of A Severely Deformed Metallic Glass, Phys. Rev. Lett. **112**, 135501 (2014).

[55] Yu. P. Mitrofanov, M. Peterlechner, S. V. Divinski, and G. Wilde, Impact of Plastic Deformation and Shear Band

Formation On the Boson Heat Capacity Peak of A Bulk Metallic Glass, Phys. Rev. Lett. **112**, 135901 (2014).

[56] R. Hubek, M. Seleznev, I. Binkowski, M. Peterlechner, S. V. Divinski, and G. Wilde, The impact of micro-alloying on relaxation dynamics in $Pd_{40}Ni_{40}P_{20}$ bulk metallic glass, J. Appl. Phys. **124**, 225103 (2018).

[57] V. A. Khonik, N. P. Kobelev, Yu. P. Mitrofanov, K. V. Zakharov, and A. N. Vasiliev, Boson heat capacity peak in metallic glasses: Evidence of the same defect-induced heat absorption mechanism in structurally relaxed and partially crystallized states, Phys. Status Solidi RRL **12**, 1700412 (2018).

[58] Yu. P. Mitrofanov, A. S. Makarov, G. V. Afonin, K. V. Zakharov, A. N. Vasiliev, N. P. Kobelev, G. Wilde, and V. A. Khonik, Relationship between the boson heat capacity peak and the excess enthalpy of a metallic glass, Phys. Status Solidi RRL **13**, 1900046 (2019).

[59] W. Schirmacher, T. Scopigno, and G. Ruocco, Theory of vibrational anomalies in glasses, J. Non-Cryst. Solids **407**, 133 (2015).

[60] B. B. Laird and H. R. Schober, Localized Low-Frequency Vibrational Modes in A Simple Model Glass, Phys. Rev. Lett. **66**, 636 (1991).

[61] H. R. Schober and B. B. Laird, Localized low-frequency vibrational modes in glasses, Phys. Rev. B **44**, 6746 (1991).

[62] S. R. Elliott, A unified model for the low-energy vibrational behaviour of amorphous solids, Europhys. Lett. **19**, 201 (1992).

[63] A. V. Granato, Interstitial resonance modes as a source of the boson peak in glasses and liquids, Physica B **219–220**, 270 (1996).

[64] S. N. Taraskin, Y. L. Loh, G. Natarajan, and S. R. Elliott, Origin of the Boson Peak in Systems with Lattice Disorder, Phys. Rev. Lett. **86**, 1255 (2001).

[65] H. Shintani and H. Tanaka, Universal link between the boson peak and transverse phonons in glass, Nat. Mater. **7**, 870 (2008).

[66] W. Schirmacher, B. Schmid, C. Tomaras, G. Viliani, G. Baldi, G. Ruocco, and T. Scopigno, Vibrational excitations in systems with correlated disorder, Phys. Status Solidi C **5**, 862 (2008).

[67] A. I. Chumakov, G. Monaco, A. Monaco, W. A. Crichton, A. Bosak, R. Rüffer, A. Meyer, F. Kargl, L. Comez, D. Fioretto, H. Giefers, S. Roitsch, G. Wortmann, M. H. Manghnani, A. Hushur, Q. Williams, J. Balogh, K. Parliński, P. Jochym, and P. Piekarz, Equivalence of the Boson Peak in Glasses to the Transverse Acoustic Van Hove Singularity in Crystals, Phys. Rev. Lett. **106**, 225501 (2011).

[68] A. I. Chumakov, G. Monaco, A. Fontana, A. Bosak, R. P. Hermann, D. Bessas, B. Wehinger, W. A. Crichton, M. Krisch, R. Rüffer, G. Baldi, G. Carini Jr., G. Carini, G. D'Angelo, E. Gilioli, G. Tripodo, M. Zanatta, B. Winkler, V. Milman, K. Refson, M. T. Dove, N. Dubrovinskaia, L. Dubrovinsky, R. Keding, and Y. Z. Yue, Role of Disorder in the Thermodynamics and Atomic Dynamics of Glasses, Phys. Rev. Lett. **112**, 025502 (2014).

[69] Y. Wang, L. Hong, Y. Wang, W. Schirmacher, and J. Zhang, Disentangling boson peaks and Van Hove singularities in a model glass, Phys. Rev. B **98**, 174207 (2018).

[70] J. Yang, Y.-J. Wang, E. Ma, A. Zaccone, L. H. Dai, and M. Q. Jiang, Structural Parameter of Orientational Order to Predict the Boson Vibrational Anomaly in Glasses, Phys. Rev. Lett. **122**, 015501 (2019).

[71] B. Huang, Z. G. Zhu, T. P. Ge, H. Y. Bai, B. A. Sun, Y. Yang, C. T. Liu, and W. H. Wang, Hand in hand evolution of boson heat capacity anomaly and slow β-relaxation in La-based metallic glasses, Acta Mater. **110**, 73 (2016).

[72] V. T. Borisov, V. M. Golikov, and G. V. Scherbedinskiy, Connection between diffusion coefficients and energies of grain boundaries, Phys. Met. Metallogr. **17**, 80 (1964).

[73] D. Gupta, Influence of solute segregation on grain-boundary energy and self-diffusion, Metall. Trans. A **8**, 1431 (1977).

[74] A. Stukowski, Computational analysis methods in atomistic modeling of crystals, JOM **66**, 399 (2014).